PRECISE CELLO BOWING PENDULUM

Robert Mores

Faculty Design Media Information
University of Applied Sciences Hamburg, Germany
robert.mores@haw-hamburg.de

ABSTRACT

A cello bowing pendulum for precise measurement of physical parameters of bowing is presented. It is designed to hold and play bows of any style and to perform the bowing on a strict line. Such a strict line follows the bowing paradigm of musical play but also eases the instrumentation of the applied bowing forces. Two eccentric suspensions translate the initially circular track of a gravity pendulum into the desired straight line. An adjustable fraction of the weight serves as bow force, while the stringed cello is resting beneath the pendulum on a weighing scale which measures this bow force. The tractive force for bowing and the bow force are orthogonally arranged and can be adjusted and measured with centinewton precision. Secondly, bow velocity is not predefined by a driving entity but is controlled by the slip-stick interaction. A potential tractive force is intentionally combined with a damping unit so that the resulting mechanical impedance will instantaneously adapt to what the actual slip-stick process recommends including a resulting bow velocity. This adaptive operation is similar to what musicians sense during bowing and therefore appears to be a valid approach for related performance-based studies of musical acoustics. Such adaptive operation also appears to be preferable for investigations of bifurcation regimes, of reciprocal inter-instrument pitch-synchronization, of physical slip-stick interaction parameters and of maximum and minimum bow force. The paper contains the pendulum construction principle, operational modes and ranges as well as first results from regime transitions.

1. INTRODUCTION

Aim of the instrumentation is to facilitate measurements on slip-stick interaction in a valid and reliable form. Target investigations are (i) bow force limits, (ii) susceptibility to external factors, for instance inter-instrumental synchronization, (iii) characteristics of regimes and their stability.

For these fields of exploration, bowing should not be stimulated by a machine with fixed parameters of force and velocity. Electrical motors or comparable driving entities usually feature the property of high mechanical impedance. Such high-impedance predetermined bow driving is insensitive to what happens at the bowing point. This compares to what takes place when a totally inexperienced person bows a string the first time. The produced sound testifies non-optimal or non-typical operation, there is little susceptibility to sense the driving parameters necessary for a favourable sound. In terms of validity it is desirable to simulate what experienced musicians do when they sense the bow-string contact-point. Musicians will adapt their playing according to the response they feel in their hand and arm. A mechanical bowing installation with adaptive driving parameters is expected to reveal the physical parameters relevant to musical play.

The range of earlier bowing machines is diverse. Lawgreen (1980) used an electrical motor for propulsion of a wagon which holds the bow and controls the direction of bowing. Pickering (1991) started with a similar idea but used a grooved wheel to guide the bow in operation. The wheel was also used to define the bow force while investigating local temperature at the contact-point. Cronhjort (1992) used the drive system of a wire printer for propulsion and direction control. The construction, which only facilitates measurements on violins, as been used by Schoonderwaldt et al. (2008) to investigate bow-force limits. Schumacher and Garoff (1996) also used a motor-driven bow and a construction with micrometer screws to define bow pressure. With this construction Woodhouse et al. (2000) measured friction force with the help of force transducers at the string termination points. Galluzzo and Woodhouse (2014) presented yet another construction to investigate onsets. The heavy-load machine controls bow force and velocity.

These constructions have in common that they drive the bow or its substitute, a rod, by some kind of motor. Motors usually have a high mechanical impedance to perform their task. A high impedance, however, implies, that the driving motor is not necessarily susceptive to what happens to a load when moved or driven in any kind. High impedance together in combination with predefined velocity or acceleration raises issues of validity when exploring slip-stick interaction:

a) Parameter dynamics between onset and steady-state tones. For steady-state tones and the related quasi stable energy flux the possibly measured friction force translates to acoustic radiation and heat. During onset, however, the measured friction force additionally feeds the process of building up the energy for the starting string oscillation. This additional energy necessary to build up the oscillation is felt by a musician in terms of a tactile resistance, which he or she will adapt to via increased bow force and/or bow velocity.

b) The process of building up the oscillation is multi-dimensional. In order to achieve valid findings for investigated slip-stick scenarios any resulting bow force variation or velocity variation during onset should rather be modelled adequately before being used parametrically during operation. The approach here is not to model these parameters but to let the slip-stick interaction between bow and string co-define the necessary parameters, adaptively and instantaneously.

c) For understanding the stability of slip-stick regimes, it might be desirable to investigate the likelihood to reside in a certain regime or the likelihood to transit from one regime to another. Such likelihood can be measured when the driving control parameters adapt to what the slip-stick interaction wants. Such likelihood is otherwise difficult to measure, when transitions between regimes are predefined by high-impedance motion control.

d) Adaptive driving seems to be preferable also for investigations on mutual inter-instrument synchronization. Imagine an impulse of an external sound source arriving at a cello top and proceeding to the bridge and the string in the very

moment of an upcoming stick-slip transition. This impulse is likely to co-define the moment of such transition, and therefore the pitch. For such investigations the slip-stick interaction should not be ruled by predefined parameters and a high-impedance driving unit but should rather be left on its own.

e) The wolf note is another example of necessary adaption. Musicians are able to control the parameters of playing so that the wolf note can be avoided. They will sense the bow-string contact-point while controlling the parameters bow force, bow velocity, and bow-to-bridge distance to finally overcome the wolf note.

2. CONSTRUCTION PRINCIPLE

The target of the instrumentation setup is to measure physical parameters and to study slip-stick regimes in valid operational modes, i.e. in a way that comes close to what musicians do while performing. Therefore the free choice of real bows and the straight movement of such bows across their entire length are preferable. Additionally, bow-to-bridge distance, bow force, traction force, bow position and velocity should be measurable rather precisely. The main reason for preferring a pendulum arrangement against other alternatives is its potential of low friction movements. Another reason is its potential to use geometric principles for achieving steady bow forces across the entire bow length.

2.1 Geometry of height compensation

A conventional gravity pendulum inherently implies circular movements, and the centre of mass is elevated at its points of return relative to its middle position. This factor at first aggravates the target of straight movements. However, with an eccentric suspension *(ES)* the initially circular path can be converted into a straight path, at the point of attachment, see point *A* of *ES* along its movement across the positions *left* to *middle* to *right*, Fig. 1. The straight path corresponds to a circle of infinite radius, and the construction principle shown here is restricted to using an *ES* with a height to base line ratio of 1/2, see unit size *a* in Fig. 1. The pendulum requires the use of two rods or strings, one from *O1* to *B* and one from *O* to *C*. The left side of the Figure shows the construction principle using dividers, and the right side assists the analytical solution.

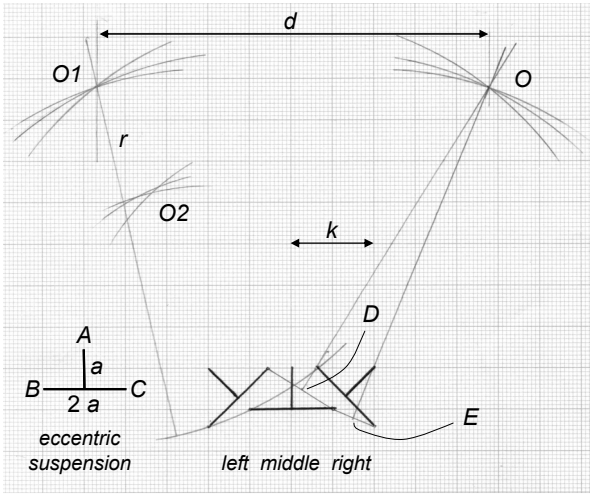

Figure 1: Construction principle for a pendulum of virtually infinite radius.

Construction with dividers: point *B* of the *ES* must follow a circular line, therefore point *B* in the *left*, *middle* and *right* position of *ES* is equidistant to the center *O1*. Reversely constructed, the circles around *B* of the *ES* in the three positions must intersect at *O1*. Likewise, the circles around *C* of the *ES* in the three positions deliver *O*. However, while constructing with dividers, the intersection of all three circles can be found for quite a range of radius *r* due to the limited precision of instruments. Out of that range, the three intersections of the three circles will not coincide, see area at *O2* in the Figure. The true *r* remains uncertain with this construction method, but a sufficiently accurate *r* can be found for an instrumentation setup.

Analytical solution: the range of operation, i.e. point *A* in *ES* strictly follows a straight line, is defined in terms of *k* multiples of *a*, precisely, $2 \cdot k \cdot a$. For the application, the bow length should be less than the total range of operation $2 \cdot k \cdot a$. While the pendulum will be able to continue the desired movement slightly beyond the indicated end positions *left* and *right*, these end positions are preferred for ease of use in an analytical approach. Furthermore, point *C* in the middle position of *ES* is the origin of the Cartesian coordinate system, normalized to the fundamental size *a* in *ES*. This setup delivers three coordinates.

$$\begin{array}{lll} C \text{ at } ES \text{ in } \textit{left} \text{ position} & x = a \cdot \left(\sqrt{2} - 1 - k\right) & y = a \\ C \text{ at } ES \text{ in } \textit{middle} \text{ position} & x = 0 & y = 0 \\ C \text{ at } ES \text{ in } \textit{right} \text{ position} & x = a \cdot (k - 1) & y = a \cdot \left(1 - \sqrt{2}\right) \end{array} \quad (1)$$

Please note that a general analytical solution is followed here, even though the illustration only shows the case of $k = 2$. The lines between these positions and the corresponding radii form isosceles triangles of individual heights, which are oriented perpendicular to mentioned lines and which intersect at center *O*, see Figure 1. Only two interceding heights of triangles are needed to determine the coordinates of *O*. This relation can be used for construction. Using this relation for the analytical solution requires determination of positions *D* and *E*.

$$\begin{array}{lll} D & x = a/2 \cdot \left(\sqrt{2} - 1 - k\right) & y = a/2 \\ E & x = a/2 \cdot (k - 1) & y = a/2 \cdot \left(1 - \sqrt{2}\right) \end{array} \quad (2)$$

These positions together with the slope of the heights of the two selected triangles

$$\begin{array}{ll} \text{slope of the line } \overline{DO} & k + 1 - \sqrt{2} \\ \text{slope of the line } \overline{EO} & k - 1 \,/\, \sqrt{2} - 1 \end{array} \quad (3)$$

form the functions

$$\begin{aligned} f_{DO}(x) &= a/2 \cdot \left[1 + \left(k + 1 - \sqrt{2}\right)^2\right] + a \cdot \left(k + 1 - \sqrt{2}\right) \cdot x \\ f_{EO}(x) &= a/2 \cdot \left[1 - \sqrt{2} + (k-1)^2 \,/\, \left(1 - \sqrt{2}\right)\right] + a \cdot k - 1 \,/\, \sqrt{2} - 1 \cdot x \end{aligned} \quad (4)$$

Solving these equations for the intersection of these functions will deliver the coordinates of center *O*, where the *x*-coordinate co-determines half of the distance *d* between *O* and *O1*, $d = 2 \cdot a \cdot (1 + x)$, which is necessary for the physical construction of the pendulum. The radius of the notation of *O* in polar coordinates directly delivers the radius *r* of the pendulum (remember that the origin of the coordinate system is at *C* of *ES* in the middle position due to the a priori definition). The radius *r* grows over-proportionally with *k* due to the quadratic components in the offsets in f_{DO} and f_{EO}, see Figure 2. The construction example in Figure 1 uses $k = 2$ and therefore

r = 8.69 a. For the implementation of a cello bowing pendulum, one might choose the parameters a = 12 cm and k = 3.5 to obtain an operating range of 84 cm, radius r = 2.32 m and the distance d = 1.3 m.

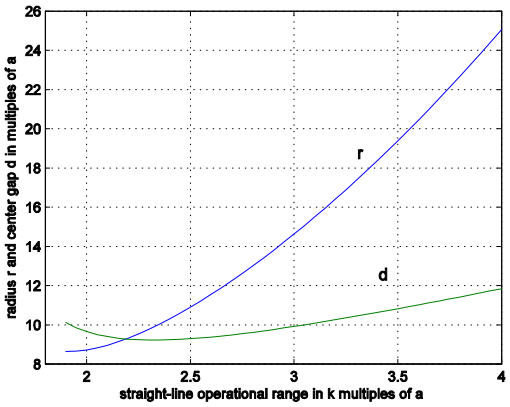

Figure 2: Pendulum geometry as derived from (4), required radius r and center gap d in multiples of basis width a versus the pendulum's maximum straight-line operational range in k multiples of basis width a.

Figure 3 illustrates the overall principle of the bowing pendulum. Two of the described *ES* systems (*ES* and *r* drawn to scale in units of a = 12 cm) are employed to hold the bow-mounting device of mass *M1* at both its ends, see *strings b* and *c*. Both ends of this device are guided on a straight line by construction, and so is the bow-mounting device. Note, that this straight line and traction forces applied through *strings d* and *e* are arranged orthogonally to the direction of gravity, which translates to the direction of bow force.

2.2 Weight compensation

The mass of the device, *M1*, emulates the mass of a cellist's arm in the range of 3 to 4 kg. It follows the straight line paradigm and its level above ground will not change. Therefore this mass will not contribute to variations of the potential energy and associated restoring forces. However, the two *ES* and the rods or strings holding them still follow a circular line of a conventional pendulum and therefore contribute to variations of potential energy. Even though the mass of these parts is only a small fraction of *M1* the pendulum will still target the middle position from either side, effectively representing a residual restoring force. This residual force disturbs the aim to operate an instrumentation setup at well definable forces and it aggravates precise measurement of these forces. Therefore, the residual force is compensated for by a counter-pendulum and its mass *M3* which is attached to *M1* by *string d*, see Figure 3. In effect, the pendulum can now be positioned at any position within its $2 \cdot k \cdot a$ range of operation without facing any restoring forces, it will simply remain where positioned.

2.3 Bow force adjustment and bow elasticity compensation

While mass *M1* is principally held by the pendulum, an adjustable fraction of its weight serves as bow force. The bow force is adjusted by fine tuning of the length of the *strings b* and *c*. Length variations of 1 mm correspond to bow force variations of several Newton in the implemented system while thin steel strings of length r are used to hold the two *ES* and the attached mass *M1*. Such length variation will not hamper the mentioned orthogonal arrangement of applied forces given a sufficient width of the total arrangement, here 6 m, not drawn to scale in Figure 3.

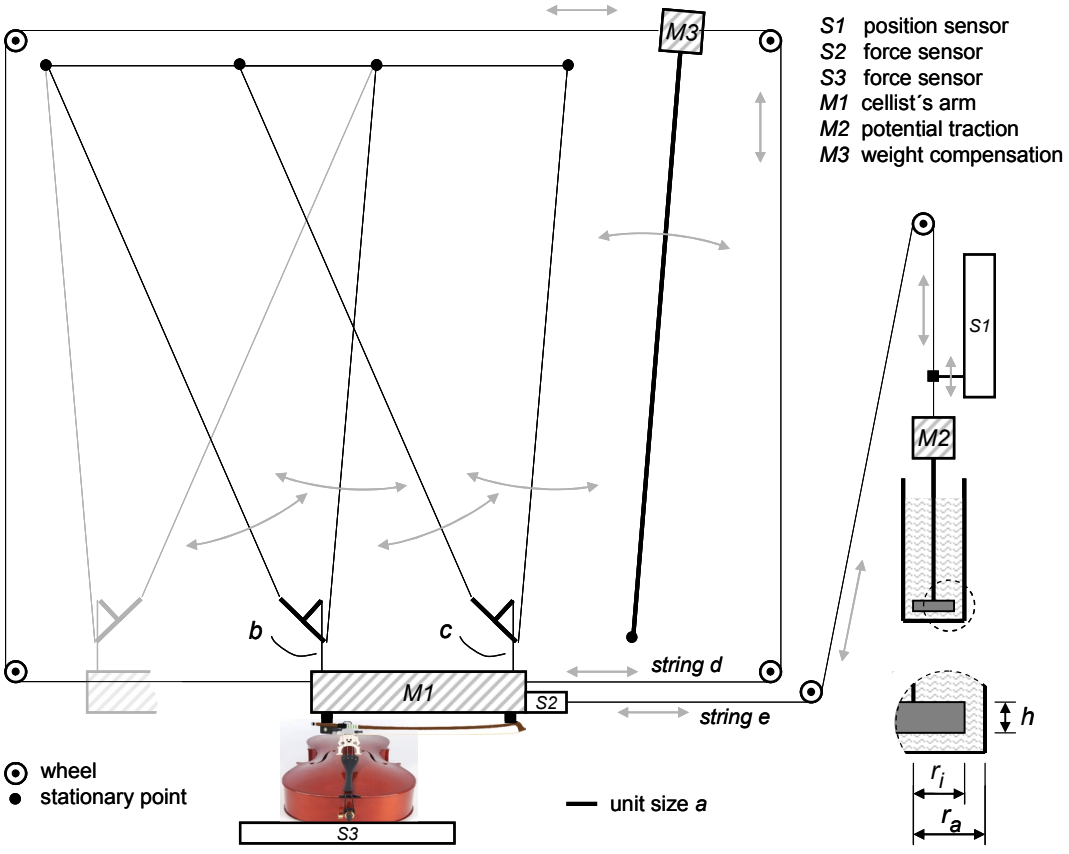

Figure 3: Schematic of the pendulum's total arrangement.

Bow force adjustments directly translate to the attached bow at its rather stiff ends, frog and tip. Along the bow hair, however, the force will be lower than at its ends when following the straight line paradigm and given the elasticity of bow and hair. In the middle section the bow will usually have to *dive deeper* towards the strings as compared to the end sections to achieve comparable forces. This can be observed while bowing. Such desirable diving can be applied, when relaxing the straight line paradigm. While point *A* of *ES* follows a straight line, see Figure 1, other points along the section from *A* to the base line *BC* will follow a circle the radius of which will range from infinity—close to *A*—to fractions of *r* depending on *k*—close to the base line *BC*. Therefore, altering the height of *ES* will allow to adjust a desirable curvature that would facilitate steady-state bow forces across the entire length for individual bows. In the implemented setup the height of *ES* can be lowered by up to 10% of its target value which comfortably allows to do all necessary adjustments. Note that this kind of adjustment also relaxes the need of precisely finding or precisely implementing the radius *r*.

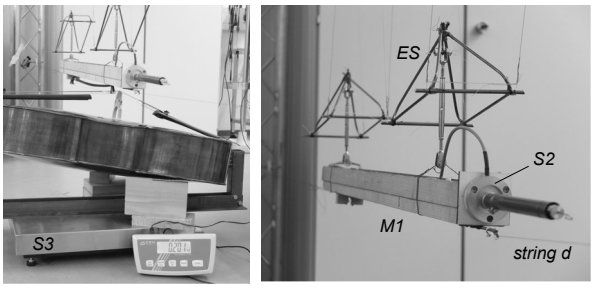

Figure 4: Implemented pendulum, in operation (left) and the compensated pendulum (right).

2.4 Adaptive driving entity

The introduction listed several issues of validity why it is not preferable to simply use a strong motor to apply the necessary traction force to the bow. The disturbing property is the high impedance. A motor of such high impedance is unlikely to adapt to the dynamics of a low-impedance load.

For the purpose of the targeted investigations, the driving unit is of low impedance and designed to adapt to the dynamics of the load. Its impedance will decrease with increasing bow velocity, similar to what a musician experiences.

The Hagen-Poiseuille relation for fluids is adapted to the laminar flow of a fluid along a non-rotating cylinder (Petzoldt 2015). A cylinder of height h and radius r_i is moved in a cylindric vessel of radius r_a, see Figure 3. This geometry is used in the derived Hagen-Poiseuille relation and delivers the force-velocity relation in dependence of the fluid's viscosity η in Pa·s

$$\eta = \frac{F_d}{2 \cdot \pi \cdot h \cdot v} \cdot \left[\ln\left(\frac{r_a}{r_i}\right) + \frac{r_i^2 - r_a^2}{r_i^2 + r_a^2} \right] \qquad (5)$$

while using SI units. This formula considers shear friction only and no turbulence and will therefore predict for low velocity only.

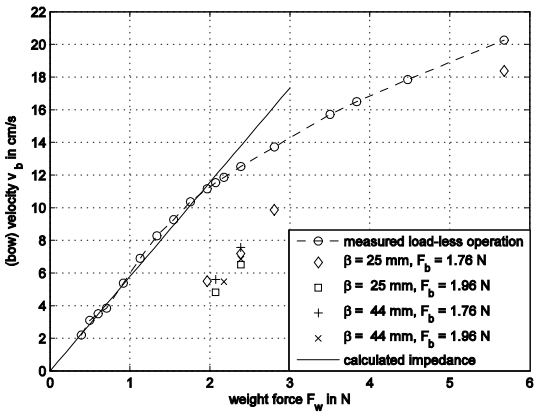

Figure 5: measured and calculated impedance of the driving entity for load-less operation, and measured velocity-weight-force relations for some load cases on the open D-string of a cello.

Figure 4 illustrates the source impedance for a damping device with r_a = 2 cm, r_i = 1.6 cm, h = 0.01 m, and filled with water, η = 1 Pa·s at 20 °C. The prediction roughly matches the measured values for low velocity. This velocity versus force curve indicates the velocity that is reached with a certain weight force represented by $F_w = M2 \cdot g$. This is the point of equilibrium where the weight force F_w is equivalent to the shear friction force F_d of the fluid. In other words, this curve represents the source driving characteristics without any load (*string e* is disconnected). In the case of a load, for example the few individual cases at F_w = 2 N and v_b = 5 cm/s, the potential force F_w will be in equilibrium with the sum of F_d and F_t, with F_t being the tractive force applied to the bow unit. F_d for the achieved bow velocity is now somewhat less than 1 N, and F_t is approximately 1.2 N. Variations in the slip-stick process will translate to variations of F_t and the corresponding bow velocity will adapt. The slope of such adaption is roughly 6 cm/s per N. The adaption is also observable for the four slightly different load cases leading to slightly different bow velocities at the given weight force F_w = 2.4 N. Load cases are denoted by the bow-to-bridge distance β relative to the string length and by the bow force F_b.

Range and relations of F_w and velocity reasonably relate to the impedance of a human arm. For a wider view of human body parts impedance see Mizrahi (2015). The velocity-dependent force can well be felt when manually driving *M2*, and the response feels like the resistance when bowing a cello string.

3. PARAMETER INSTRUMENTATION

3.1 Sensors, signaling and precision

Three parameters are measured in the system simultaneously. Sensor *S1* measures the position s_b of the bow. Bow velocity v_b and bow acceleration a_b can be derived from s_b.

Sensor *S2* measures the tractive force F_t applied to the bow unit via *string e*. *S2* does not measure tractive forces applied via *string d*, which are meant to compensate the two-sided residual restoring forces of the pendulum. However, the four wheels used to guide *string e* constitute a little frictional force when in motion, F_p , see Figure 5. F_p is kept very low, in the range of 0.1 ... 0.3N, depending on adjustments of tension in *string d*. F_p is also very stable across velocity v_b and across position s. F_p can be measured separately for each session to be used for post-calibration of data. The pendulum can be moved in a load-less mode of operation, i.e. without any contact between bow and instrument, and the measured tractive force F_t will directly

correspond to the pendulums friction F_p . For measurements of the static or dynamic friction between bow and string, F_f, sensor *S2* will finally capture F_f only indirectly, $F_f = F_t - F_p$. In cases of non-stationary velocity, the acceleration force $F_a = M1 \cdot a$ (*a* now stands for the acceleration and not for the unit length in *ES* geometry) has to be accounted for, see the arrow shaded in gray in Figure 6. Such non-stationary operations require an $F_f = F_t - F_p - F_a$ correction term.

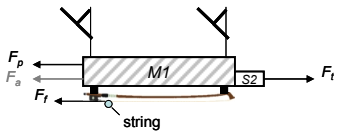

Figure 6: Frictional force at the bow F_f in relation with traction force F_t, frictional force of the compensation strings F_p, and possibly acceleration force F_a.

Sensor *S3* measures the bow force, F_b. Indeed, the high-precision industrial weigh scale measures the entire cello including the mounting jig used to hold the cello. However, relative measurements capture the additional bow force and its variations. Remember, that *string e* and therefore the force F_t are arranged strictly orthogonal to the gravitational force F_b so that even the momentum caused by F_t will not alter measurements of F_b.

All sensor signals are electrically converted prior to sampling: The DC signal from *S1* is converted to frequency, the *S2* Wheatstone bridge is operated with AC and the *S3* weighting scale signal is converted to frequency. All signals are captured at f_a = 192 kHz. For sensor types see appendix.

Precision is limited mechanically and electrically. The precision of position s_b is limited by the elasticity of *string e*, by limited precision of *S1*, and by limited stability of the VCO. The precision of F_f is limited by the contribution of F_p in F_t and by an initial calibration procedure. The precision of F_b is limited by the precision and linearity of the weighting scale and by the drift of the VCO. For details see Appendix A. Table 1 lists the overall maximum errors.

Table 1: Parameters measured and related maximum errors

physical property		sensor	maximum error
s_b in cm	bow position	*S1*	± 0.18 cm
v_b in cm/s	bow velocity	derived from s_b	± 0.025 cm/s
F_t in N	traction force	*S2*	± 0.15 N ± 1 %
F_b in N	bow force	*S3*	± 0.11 N

In terms of dynamical response, sharp impulses were applied to the sensors and the individual response time measured after all procedural steps of conversion, analysis and normalization. More precisely, a traction force impulse of 10 N has been applied to sensor *S2* (half of its operational range but three times the range needed in instrumentation), a weight impulse of 10 N has been applied to *S3* (1/60 of its operational range but twice the range needed for instrumentation), and a displacement step of 3 cm has been applied to *S1* (only 1/20 of its operational and instrumental range due to impedimental mass load). The response time $T_{10/90}$ is measured at the 10 % and 90 % fractions of the total impulse or step total amplitude and is less than 10 ms in all cases, see Table 2.

Table 2: Parameter measurement dynamic response

physical property		sensor	impulse / step	$T_{10/90}$
s_b	bow position	*S1*	3 cm step	~6 ms
F_t	traction force	*S2*	10 N impulse	~0.8 ms
F_b	bow force	*S3*	10 N impulse	~8 ms

For sound recording a piezo of 1 gram weight is directly mounted to the bridge.

3.2 Operational range

The implemented construction facilitates bowing of all four classical instruments from violin to double bass. Bow velocity can be comfortably adjusted from zero to v_b = 30 cm/s. Bow forces can be adjusted from zero to 5 N and is typically limited by the bow stiffness. Adjustments allow to enforce stationary bow forces along s_b within a corridor of ± 0.01 N (can be monitored directly at *S3* even though the captured signal has the maximum error as outlined in Table 1) but also gradients of F_b. The bow-bridge-distance can be adjusted and measured in the submillimeter range. The bow in motion maintains a predefined track sufficiently well even though there is no external force to keep the targeted distance to the bridge. Note that the forces along the long *strings e and d* have only little potential of guiding any direction. Such stability of distance is not surprising and cellists know that shifting the bow towards a different β requires to resolutely change the bow-string angle.

3.3 Compact data representations

For meaningful and sparse representation of data, signals are averaged across non-overlapping windows of 12.5 ms. This is about the time span of one slip-stick period on the lower strings of a cello and of a few slip-stick periods on the higher strings. The recorded sound is analyzed in terms of pitch frequency using the YIN algorithm (Cheveigné and Kawahara, 2002) in order to classify between Helmholtz motion and non-Helmholtz regimes. A bow stroke finally generates data tuples of 200 to 1500 times four numbers, depending on bow velocity.

4. REGIME-TRANSITION EXAMPLE

Figure 7 represents an example of operation where the bow force is intentionally adjusted to gradually decline along the bow position s_b. The two sound samples are provoked by varying the weight force F_w which is not the measured traction force F_t in the trace below.

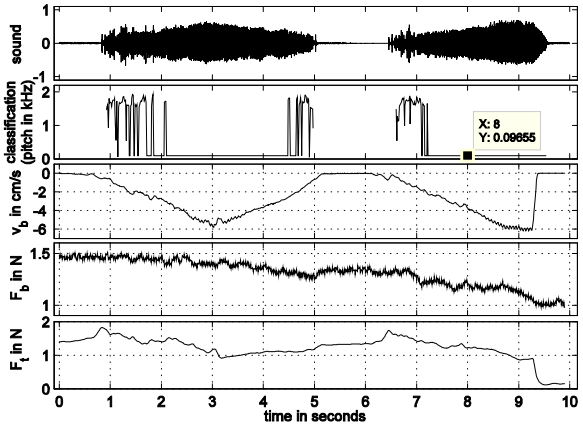

Figure 7: Traces of parameters for transitions between bifurcation and Helmholtz motion (resolution 12.5 ms), from the top: sound, classification (Helmholtz-motion at nominal pitch of open G string versus bifurcation at higher pitches), bow velocity (v_b<0 for upstroke), bow force, and traction force.

Figure 8 represents the populations of bow velocity v_b versus bow force F_b. Using the classification data for Helmholtz versus non-Helmholtz motion reveals the related parameter ranges necessary to establish either regime. Three features can be observed here. (i), there are gaps between the regimes,

suggesting, that there is no smooth transition but rather a jump from one regime to the other. This gap denotes the maximum bow force and can be extracted from the data. (ii), there are also visible gaps within a class, suggesting that there exist subclasses of stability with related preferred bowing parameters. Obviously, the slip-stick process co-moderates the resulting velocity for a given bow force. Note that these populations can be disclosed by the adaptive driving unit only. (iii), a hysteresis can be observed while plotting Figure 8 in timely sequence. This further endorses the observation of stability of regimes, or, in other words, the hesitation to transit to another regime.

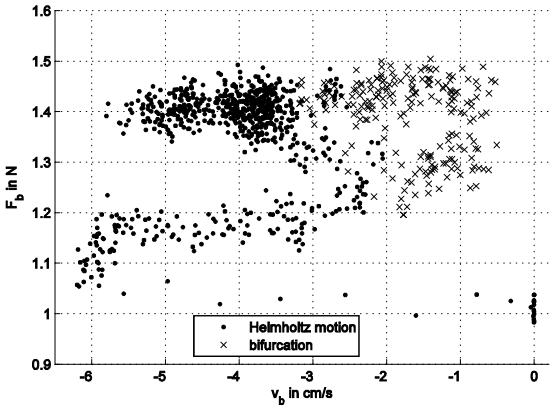

Figure 8: Bow force versus bow velocity populations for Helmholtz motion (dots) and for bifurcation-regimes (cross), same data as in Figure 7, populations reveal visible (i) gaps between regimes, (ii) gaps within regimes, (iii) hysteresis between transitions.

5. SUMMARY

A pendulum is presented that allows precise measurement of bow velocity and bow forces. Bow forces comply both traction force and bow force. Measurements can be taken during the bowing of all kinds of stringed instruments and all styles of bows. While restoring forces of the pendulum are compensated for, precise measurement of mentioned bow forces is facilitated at maximum errors of about 0.1 N. The dynamic response time is less than 10 ms for all parameters measured. An example of transitions between Helmholtz motion and bifurcation regimes demonstrates that stability issues can now be explored which was not possible with earlier constructions. This is due to the adaptive bow driving mechanism which emulates the musician's sensitivity with respect to the bow-string interaction and resistance. The pendulum is fully described to facilitate reconstruction by others, but researchers are also welcome to directly use the existing construction.

6. REFERENCES

Cheveigné, A., H. Kawahara: Yin, a fundamental frequency estimator for speech and music. Journal of Acoustical Society of America, 111 (2002) 1917–1930.

Cronhjort, A.: A computer-controlled bowing machine (MUMS). STL-QPSR 33 (1992) 61–66.

Galluzzo, P. M., J. Woodhouse: High-performance bowing machine tests of bowed-string transients. Acta Acustica united with Acustica 100 (2014) 139–153.

Lawgren, B.: On the motion of bowed violin strings. Acustica 44 (1980) 194–206.

Mizrahi, J.: Mechanical Impedance and Its Relations to Motor Control, Limb Dynamics, and Motion Biomechanics. J. Med. Biol. Eng. 35 (2015) 1–20.

Petzoldt, T.: Ringspaltgleichung für Viskosimeter (equations for annular gaps in viscometers, with derivation), published on the IMETER company webpage, URL http://www.imeter.de/adienstleistungen/dienstviskositaet/75-viskositaet-im-ringspalt.html, downloaded June 16, 2015.

Pickering, N. C.: A new light on bow action. Journal of the Violin Society of America 11 (1991) 83–92.

Schoonderwaldt, E., K. Guettler, A. Askenfelt: An empirical investigation of bow-force limits in the Schelleng diagram. Acta Acustica united with Acustica 94 (2008) 604–622.

Schumacher, R. T., S. Garoff: Bowing with a glass bow. Journal of the Catgut Acoustical Society 3 (1996) 9–17.

Woodhouse, J., R. T. Schumacher, S. Garoff: Reconstruction of bowing point friction force in a bowed string. Journal of Acoustical Society of America 108 (2000) 257–368.

7. APPENDIX

These are more details on sensor devices and related error components for the three physical properties measured.

For the Novotechnik TP1-800 , representing *S1*, non-linearity, hysteresis, resolution and repeatability amount to ± 0.5 mm. Signal conversion and post-sampling processing introduce an additional error of ± 0.1 mm. Calibration introduces an additional maximum uncertainty of ± 0.2 mm. Additionally, the elasticity of string *e* introduces an additional uncertainty of ± 1 mm for the given length and the range of forces applied. The total maximum error in measuring the bow position s_b is therefore ± 1.8 mm.

Note that the error for bow velocity v_b is smaller than for the position s_b since error components contributing to the absolute position error are not relevant after derivation. The limited resolution of *S3* and the signal conversion maximum error contribute most to the residual estimated uncertainty of ± 0.25 mm for the velocity v_b.

For the Burster 8520, representing *S2*, non-linearity, hysteresis and repeatability amount to ± 0.1 N. Signal conversion and post-sampling processing introduce an additional error of ± 0.05 N. Calibration introduces an additional uncertainty of ± 1% maximum. The total maximum error in measuring traction force F_t is therefore ± 0.15 N ± 1 %.

For the Kern-DE 60K1D, representing *S3*, non-linearity, hysteresis, resolution and repeatability amount to ± 0.05 N maximum. Signal conversion and post-sampling processing introduce an additional error of ± 0.04 N maximum. Calibration introduces an additional uncertainty of ± 0.02 N maximum. The total maximum error in measuring bow force F_b is therefore ± 0.11 N.